Langmuir

ARTICLE

pubs.acs.org/Langmuir

Effect of Graphite Features on the Properties of Metal−Organic Framework/Graphite Hybrid Materials Prepared Using an in Situ Process

Camille Petit, Barbara Mendoza, Deanna O'Donnell, and Teresa J. Bandosz*

The Department of Chemistry, The City College of New York and the Graduate School of the City University of New York, 160 Convent Avenue, New York, New York 10031, United States

Supporting Information

ABSTRACT: Metal−organic framework (MOF)/graphite hybrid materials were prepared using an in situ process. Graphites with various chemical and physical features were used, and HKUST-1 was selected as the MOF component. The samples (parent materials and hybrid materials) were characterized by X-ray diffraction, nitrogen sorption, scanning electron microscopy, Raman spectroscopy, Fourier transform infrared spectroscopy, and thermogravimetric analysis. Then they were tested as ammonia adsorbents in dynamic conditions. The results indicate that the functionalization of graphite is important to build the hybrid materials with synergistic properties. The lack of functional groups on graphite results in the formation of a simple physical mixture. Besides the surface chemistry of the graphitic component, the physical parameters (porosity and size of flakes) also seem to influence the formation of the hybrid materials. It is observed that the graphite particles disturb the formation of HKUST-1 and induce a different crystal morphology (more defects and increased surface roughness) than the one observed when MOF is formed in the absence of a substrate. The latter behavior causes less ammonia to be adsorbed on the hybrid materials than is expected for the simple physical mixture of HKUST-1 and graphite. The MOF structure collapses (in HKUST-1 and the hybrid materials) upon ammonia adsorption and leads to the formation of new species.

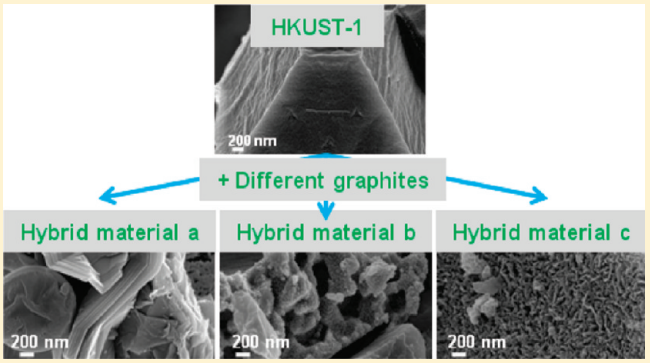

INTRODUCTION

Over the past two decades the fields of gas adsorption and catalysis have greatly benefited from the development of a class of materials called metal−organic frameworks (MOFs).[1−3] MOFs represent a class of crystalline and highly porous hybrid materials obtained by the assembly of metallic ions and organic ligands.[2,4,5] The diversity of metals and organic linkers that can be used to synthesize MOFs makes these materials highly tunable.[4,5] Besides an application in gas adsorption and catalysis, MOFs exhibit interesting properties for gas separation, gas storage, and drug delivery and could also be used as sensors (luminescent and magnetic properties).[1,2,6−11]

To drive MOFs up to the step of industrial/large-scale applications, several drawbacks/limitations must be addressed. The latter include: poor stability of selected MOFs in the presence of humidity or upon a solvent removal (one of the steps of their synthesis) and weak dispersive forces for the adsorption of small molecule gases (e.g., ammonia or hydrogen). Moreover, there is a need to produce MOFs, currently available in the form of powder, into "user-friendly" configurations (e.g., membranes, thin films, etc.). Many research efforts have focused on these issues and the deposition of MOF on various supports such as alumina,[12−17] silica,[16−18] functionalized self-assembled monolayer (SAM),[16,19] functionalized graphite,[12,20] graphite oxide (GO),[21−23] or amorphous carbon[15] have been recently reported as a way to produce MOF-based membranes or composites. These studies indicate that the functionalization of the substrate is important in the preparation of MOF-based composites. In particular, Jahan and co-workers reported the growth of MOF-5 on functionalized graphite and found that the graphite influences the crystal growth of the MOF.[20] Shekkah and co-workers, who studied the step by step grafting of a copper-based MOF on COOH-functionalized SAMs, showed that copper ions are used as linkers between the carboxyl groups of the SAMs and those of the organic ligands.[19] We have recently reported the preparation and characterization of MOF/GO composites and showed that the composites were formed via interactions between the oxygen groups of GO and the metallic centers of the MOF.[21−23] These composites showed higher ammonia and hydrogen adsorption capacities than those

Received: May 10, 2011
Revised: June 18, 2011
Published: July 14, 2011

dx.doi.org/10.1021/la2017424 | *Langmuir* 2011, 27, 10234–10242

expected for the physical mixture of MOF and GO.[23−25] This was attributed to the new pore space created at the interface between the MOF and the GO components owing to the linkages formed between the metallic centers of the MOF and the functional groups of GO.[25] Even though the chemistry of the substrate seemed to play a role in the formation of MOF-based composites, clear evidence of such effect has yet to be proposed. Moreover, the effects of the carbonaceous support's physical features on the MOF growth have not been studied.

The research presented in this paper focuses on MOF/graphite hybrid materials and it is a continuation of our previous work on MOF/GO materials. Graphites with differences in their chemical and physical features are used to prepare the hybrid materials. The MOF selected is HKUST-1 and contains copper ions as the metallic centers and molecules of benzene tricarboxylic (BTC) as the organic ligand.[26] HKUST-1 was chosen owing to its relatively easy synthesis and large porosity, and the presence of unsaturated metallic copper sites able to bind to ammonia. The samples (parent materials and hybrid materials) were characterized by various techniques and tested for ammonia adsorption in dynamic conditions. The results of this study, along with those obtained on MOF/GO composites, should bring a clearer picture of the role of the substrate's functional groups on the formation of MOF-based composites as well as an indication of the influence of the substrate's physical features. Indeed, in the case of the MOF/GO composites, formation of the composites was proposed to occur as a result of the linkages between the oxygen groups of GO and the metallic centers of the MOF.[21−23] It was suggested that these linkages were responsible for an increase in porosity in the composites compared to the parent materials. By studying hybrid materials involving MOF and graphite and comparing the results to those obtained on MOF/GO composites, we intend to clearly isolate the effect of the oxygen groups. This will provide a better understanding of their role on the porosity formation. Therefore by suppressing the effect of the GO functional groups, we can better isolate the influence of the physical parameters of graphite on the formation and structure of the resulting MOF/graphite materials.

EXPERIMENTAL SECTION

Materials. Five graphites were used to prepare the MOF/graphite composites. The first graphite, referred to as Gr1, was a synthetic material (flakes <20 μm). Another synthetic graphite (flakes ∼200 μm), referred to as Gr2, was used as received, and a part of it was subjected to energy impact milling using dense media. The process was done continuously for 48 h and resulted in the graphite called Gr3 (flakes ∼2−3 μm). Another sample, graphite Gr4, was obtained by grinding of compressed, exfoliated natural flake graphite (flakes ∼8 μm). Exfoliated graphite (flakes between 400 and 1000 μm), referred to as Gr5, was also used to broaden the spectrum of surface properties. It was obtained from graphite intercalated with sulfuric acid by heating it to 800 °C for 30 s in air atmosphere.[27] Gr1 was supplied by Sigma-Aldrich and Gr2, Gr3, and Gr4 were provided by Asbury Graphite Mills. The graphite intercalated with sulfuric acid used to obtain the exfoliated graphite, Gr5, was also provided by Asbury Graphite Mills.

HKUST-1 was prepared by mixing copper nitrate hemipentahydrate (10 g) and 1,3,5-benzenetricarboxylic acid (5 g) in *N*,*N*-dimethylformamide (DMF, 85 mL) followed by stirring and sonication for 5 min. Ethanol (85 mL) was then added to the mixture, which was then stirred and sonicated for 5 min. Finally, deionized water (85 mL) was added to the mixture and it was followed by stirring and sonication for 5 min. All crystals were dissolved at this point. The mixture was then transferred to a round-bottom flask (500 mL) and heated at 85 ° C in an oil bath. It was kept in the oil bath for 21 h under shaking (intensely for the first 4 h, and then the shaking was reduced and then stopped after 20 h). After cooling, the crystals were filtered using a Büchner funnel, washed, and immersed in dichloromethane. Dichloromethane was changed twice during three days. After filtration and washing with dichloromethane, the crystals were collected. Drying was then performed by heating the crystals at 170 °C for 28 h inside a closed filtering flask connected to an aspirator. The aspirator was used to create a vacuum inside the flask. The resulting product was kept in a desiccator and is referred to as HKUST-1.

The hybrid materials were prepared by adding a graphite powder to the well-dissolved MOF precursors and solvent mixture, which was used for HKUST-1 synthesis. The resulting mixture was sonicated for 5 min, stirred for another 30 min and then the same synthesis procedure as that for HKUST-1 was carried out. The synthesis conditions were kept the same as those used for the preparation of HKUST-1 in order to isolate the effect of the graphite component on the MOF structure. Only, the sonication time was slighlty longer in the case of the hydrid materials than for MOF to favor exfoliation of the graphite. The hybrid materials are referred to as MGr*n* with n = 1, 2, 3, 4, and 5 depending on the graphite used. The estimated graphite contents (from thermal analysis) in MGr1, MGr2, MGr3, MGr4, and MGr5 are 10.6, 10.0, 11.3, 14.9, and 3.5 wt % graphite, respectively. In the case of MGr5 where unlike the other hybrid materials the low-density exfoliated graphite was used, the difficulties in its dispersion within the HKUST-1 precursors' mixture resulted in a low content of the graphite component. The percent of graphite incorporated to the hybrid materials was measured as a weight loss between 450 and 700 °C during heating in air, which was the result of the carbonaceous phase burning.[28]

Methods. *NH_3 Breakthrough Dynamic Test.* In order to determine the ammonia breakthrough capacity, dynamic breakthrough tests were performed at room temperature. In a typical test, a flow of ammonia diluted with air went through a fixed bed of adsorbent with a total inlet flow rate of 225 mL/min and an ammonia concentration of 1000 ppm*v*. The adsorbent's bed contained about 2 cm^3 of glass beads well mixed with the amount of adsorbent required to obtain a homogeneous bed (about 60 mg). The mixture was packed into a glass column. The beads were used to avoid the pressure drop. The concentration of ammonia in the outlet gas was measured using an electrochemical sensor (Multi-Gas Monitor ITX system). The adsorption capacity of each adsorbent was calculated in mg per gram of the material by integration of the area above the breakthrough curve. The statistical error range in the adsorption capacity is about 10%. Tests in dry and wet conditions were performed by diluting the ammonia stream with either dry or moist air stream, respectively. This was done to analyze the effects of water on the adsorption capacity. After the breakthrough tests, all samples were exposed to a flow of carrier air only (180 mL/min) to impose the desorption of ammonia and thus to evaluate the strength of its retention. The suffixes -ED and -EM are added to the name of the samples after the exposure to ammonia in dry and moist conditions, respectively.

X-ray Diffraction (XRD). XRD measurements were conducted using standard powder diffraction procedures. Adsorbents (initial and exhausted) were ground with DMF (methanol for the graphite samples) in a small agate mortar. The mixture was smear-mounted onto a glass slide and then analyzed by $Cu_{K\alpha}$ radiation generated in a Philips X'Pert X-ray diffractometer. A diffraction experiment was run on standard glass slide to for the background correction.

Scanning Electron Microscopy (SEM). SEM was performed on a Zeiss Supra 55 instrument. The instrument has a resolution of 5 nm at 30 kV. Scanning was performed on a sample powder previously dried. For some samples, a sputter coating with a thin layer of gold or carbon was performed to avoid charging.

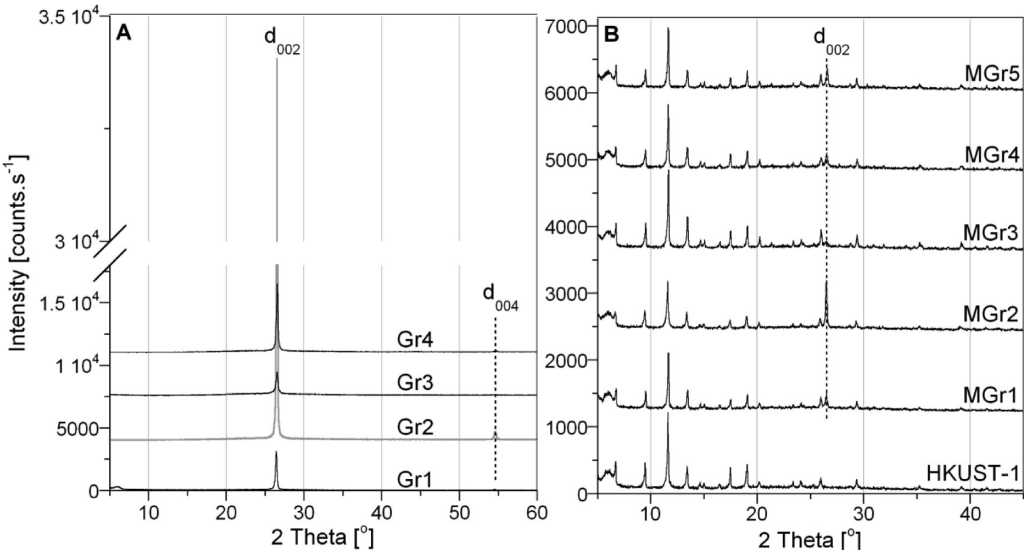

Figure 1. XRD patterns for the samples studied.

Sorption of Nitrogen. Nitrogen isotherms were measured at −196 °C using an ASAP 2010 instrument (Micromeritics). Prior to each measurement, initial and exhausted samples were outgassed at 120 °C to vacuum 10 Torr. The surface area, S_{BET}, (Brunauer−Emmet−Teller method),[29] the micropore volume, V_{mic}, (calculated from the t-plot which corresponds to the plot of the volume of N_2 adsorbed as a function of the layer thickness, "t". Extrapolation of the Y-intercept enables the determination of V_{mic}),[30] the mesopore volume, V_{mes}, (calculated as the difference between the total pore volume and V_{mic}), and the total pore volume, V_t (calculated from the volume of N_2 adsorbed at $P/P_0 = 0.985$), were calculated from the isotherms.

Potentiomtric Titration. The measurements were performed with a DMS Titrino 716 automatic titrator (Metrohm). The instrument was set at the mode when the equilibrium pH was collected. Samples (about 50 to 100 mg) were placed in a container, dispersed in NaNO3 (0.01M, 50 mL) and equilibrated overnight with the electrolyte solution. Prior to the titration with NaOH (0.1 M), the suspension was acidified to a pH of 3.20 or below by addition of HCl (0.1 M). The titration was performed in the pH range 3−10, with constant stirring and continuous saturation with nitrogen to eliminate the influence of atmospheric CO_2.

The surface properties were evaluated using potentiometric titration experiments.[31,32] Here, it is assumed that the population of sites can be described by a continuous pK_a distribution, $f(pK_a)$. The experimental data can be transformed into a proton binding isotherm, Q, representing the total amount of protonated sites, which is related to the pK_a distribution by the following integral eq 1.

$$Q(\mathrm{pH}) = \int_{-\infty}^{\infty} q(\mathrm{pH}, \mathrm{p}K_a)\, f(\mathrm{p}K_a)\, \mathrm{d}\mathrm{p}K_a \qquad (1)$$

The solution of this equation is obtained using the numerical procedure (SAIEUS),[31,32] which applies regularization combined with non-negativity constraints. Based on the spectrum of acidity constants and the history of the samples, the detailed surface chemistry can be evaluated.

Raman Spectroscopy. Raman spectra were collected on a Princeton Instruments Acton 2750 SpectroPro 0.750 m Triple Grating Monochromator fitted with an Olympus BX-51 microscope and 10× objective using a 514.5 nm Argon-ion laser with a 1200 gr/mm grating. The laser power used was 1−3 mW at the stage. To obtain adequate signal-to-noise ratio signal averaging was employed; a total acquisition of 300 s for the HKUST-1 and graphite samples and 1800 s for the MGr*n* composite samples. All reported spectra underwent baseline correction to remove fluorescence contamination and 5-point adjacent averaging smoothing. Raman intensities of the MGr*n* composite samples have been normalized to the out-of-plane ring (CH) bending mode (826 cm^{-1}) of HKUST-1, which is isolated spectrally enabling a reliable comparison of spectra. The experiments were done on the powdered samples deposited on a silicon wafer.

FT-IR Spectroscopy. Fourier transform infrared (FT-IR) spectroscopy was carried out using a Nicolet Magna-IR 830 spectrometer using the attenuated total reflectance method (ATR). The spectrum was generated, collected 16 times and corrected for the background noise. The experiments were done on the powdered samples (initial and exhausted), without KBr addition.

Thermal Analysis. Thermogravimetric (TG) curves were obtained using a TA Instruments thermal analyzer. The initial and exhausted samples were exposed to an increase in temperature (10 °C min^{-1}) while the nitrogen flow rate was held constant (100 mL min^{-1}). From the TG curves, differential TG (DTG) curves were derived.

RESULTS AND DISCUSSION

Even though the surface of the graphites used in this study was described in detail elsewhere,[27,33] we reintroduce some data in this paper in order to link these surface features to the features of the hybrid materials as well as their ammonia adsorption properties.

The XRD patterns of the parent materials and the hybrid materials are presented in Figure 1. The graphite samples exhibit a peak at about 27° which is related to an interlayer distance (d_{002}) of about 3.4 Å.[34] An additional peak at about 55° (d_{004}) is observed, mainly in the case of Gr2 and Gr4.[34] The absence of that peak (or its much lower intensity) in the case of Gr1 and Gr3 indicates the presence of structural defects in Gr1 and Gr3.[34] It has to be noted that XRD analysis was not performed on Gr5 due to the difficulties in sample preparation (Gr5 was hardly dispersible in the solvent). Nevertheless, considering the nature of Gr5 and the XRD patterns reported in the literature for other exfoliated graphites,[27] this sample should exhibit similar features; that is, peaks at about 27° and 55° from the (002) plane (from graphite) and the (004) plane, respectively. The MOF sample shows XRD pattern typical for HKUST-1.[35] On the XRD

dx.doi.org/10.1021/la2017424 |*Langmuir* 2011, 27, 10234–10242

patterns of the hybrid materials, the features of graphite and HKUST-1 are visible, which indicates the presence of the two "phases" in these materials. The trend in the intensity of the d_{002} peak from a graphite phase in the hybrid materials follows the same trend as that for the graphite samples. The results suggest that the graphite component did not prevent the formation of the MOF in the hybrid materials. However, the fact that the main peak from graphite (d_{002}) is still present on the XRD patterns of the hybrid materials indicates that a significant part of the graphite did not exfoliate during the hybrid materials preparation and these hybrid materials still contains agglomerates of graphene layers. That lack of exfoliation was expected taking into account the properties of graphites.[36] Considering Bragg's law and the Debye−Scherrer equation, the interlayer distance and the range of crystallite sizes of the hybrid materials' graphite component that did not exfoliate were calculated. The obtained values are 3.35 Å and 300−600 Å, respectively.

Even though the graphite component does not prevent the MOF formation in the hybrid materials, it apparently modifies the morphology of the crystalline structure of the MOF particles as observed in the SEM images presented in Figure 2. In the case of HKUST-1, the octahedral shape of crystals is easily recognized (Figure 2A). On the contrary, the particles of the hybrid materials (except MGr5) show a significant surface roughness and several defects. The surface of MGr3, in particular, appears as agglomerates of globular seeds as the ones observed by Spokoyny and co-workers for a zinc-based MOF (with a Tröger's base as the organic ligand).[37] As they suggested, this likely indicates the incomplete formation of the MOF component in the hybrid materials.[37] These results show that the graphites interfered with the formation of the MOF. They likely disturbed the "encounter" between the metallic units and the organic linkers in the initial stage of the synthesis, then between the seeds, and later between the aggregates of MOF. This hypothesis is supported by the fact that when only a small amount of graphite is present in the system, as in the case of MGr5, well-defined HKUST-1 crystals are formed (Figure 2G). It has to be noted as well that in the case of MGr4, stacked graphene layers are seen (as with XRD data) which confirms the fact graphite did not exfoliate. Finally, based on SEM analyses at low magnification (not shown here), the size of HKUST-1 particles and the MOF units in the hybrid materials were estimated to be close to 20 μm. However, the particles of the hybrid materials looked quite different from those of HKUST-1. They appeared more like agglomerates of smaller particles whereas, in the case HKUST-1, well-defined "block particles" with a smoother surface were visible.

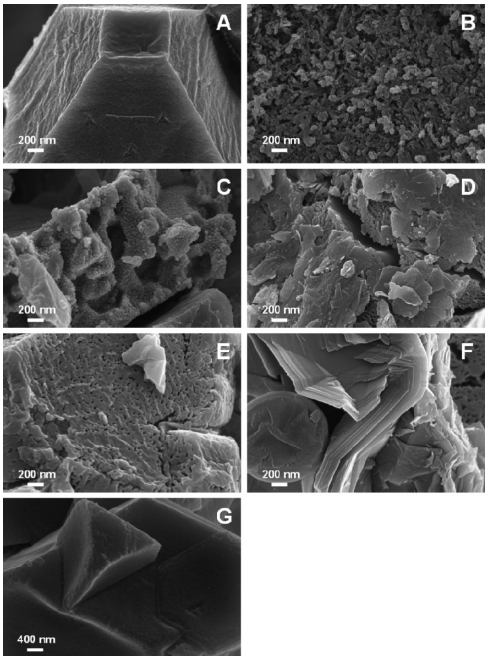

Figure 2. SEM images of (A) HKUST-1, (B) MGr1, (C) MGr2, (D) MGr3, (E and F) MGr4, and (G) MGr5.

An important aspect of adsorbents in general and MOFs in particular is the porosity of these materials. The parameters of porous structure calculated from the nitrogen isotherms are listed in Table 1 for all of the materials studied. The N_2 isotherms are available in the Supporting Information (Figure S1). Table 1 also includes the parameters of the porous structure calculated assuming a physical mixture between the MOF and the graphite components. Comparison between the measured parameters and the ones calculated enables us to identify any synergistic effect between HKUST-1 and graphite. Although Gr1 and Gr2 are nonporous materials, Gr3 exhibits a quite high surface area and pore volume considering the nonporous nature of the graphite materials in general (222 $m^2\ g^{-1}$ and 0.334 $cm^3\ g^{-1}$). The porosity of Gr4 and Gr5 are intermediate between those of Gr1 and Gr3 samples. HKUST-1 has a surface area of 984 $m^2\ g^{-1}$ and a total volume of pores of 0.514 $cm^3\ g^{-1}$. These values are similar to those reported in our previous study.[22] The porosity of the hybrid materials is in the range of that of the MOF, however, a

Table 1. Parameters of the Porous Structure Derived from the Nitrogen Isotherms at −196 °C for the Samples Studied before and after Exposure to Ammonia as well as the Parameters Calculated for the Physical Mixture (H)

sample	S_{BET} (m^2/g)	V_t (cm^3/g)	V_{meso} (cm^3/g)	V_{mic} (cm^3/g)	V_{mic}/V_t	S_{BET}H (m^2/g)	V_tH (cm^3/g)	V_{mic}H (cm^3/g)
Gr1	0.4	0.021	0.019	0.002	0.09			
Gr2	0	0	0	0	0			
Gr3	222	0.334	0.239	0.095	0.28			
Gr4	24	0.035	0.036	0.009	0.26			
Gr5	28	0.071	0.061	0.010	0.14			
HKUST-1	984	0.514	0.040	0.474	0.92			
MGr1	917	0.478	0.031	0.447	0.94	880	0.462	0.424
MGr2	912	0.471	0.027	0.444	0.94	886	0.463	0.427
MGr3	889	0.501	0.086	0.415	0.83	900	0.494	0.431
MGr4	905	0.490	0.066	0.424	0.87	841	0.443	0.405
MGr5	998	0.523	0.041	0.482	0.92	951	0.498	0.458

dx.doi.org/10.1021/la2017424 |*Langmuir* 2011, 27, 10234–10242

Table 2. Amount of Functional Groups Determined by Potentiometric Titration (in mmol/g) for the Graphite Samples and Graphite Oxide

	$pK_a < 7$	$pK_a < 7$	total
Gr1	0.147	0.017	0.164
Gr2	0.028	0.067	0.095
Gr3	0.120	0.108	0.228
Gr4	0.029	0.032	0.061
Gr5	0.200	0.720	0.920
GO	0.517	1.983	2.560

slight decrease is found (except for MGr5) due to the addition of low- or nonporous graphite. The parameters of porous structure calculated for the physical mixture are similar to those actually measured (less than 8% change) or lower (MGr3 sample). Unlike in the case of MOF/GO composites,[22] no measurable enhancement in the porosity compared to the physical mixture is observed. It was indicated that the enhancement in the porosity of the MOF/GO composites was caused by the formation of linkages between the GO functional groups and the metal centers of the MOF which led to the additional pore space. In the case of graphite materials, on which likely only few or no functional groups are present, this type of interactions with the MOF cannot occur and thus the creation of a new porosity at the interface MOF/graphite is very limited. That lack of the increase in the porosity for MOF/Graphite hybrid materials supports our previous findings reported for the MOF/GO composites.[22] Indeed, the presence of oxygen groups on GO enabled chemical bindings between the MOF units and GO, resulting in an increase in the porosity (see ref 22). On the contrary, when the oxygen groups are absent (case of the present study), chemical binding cannot occur and thus no increase in the porosity is observed. The fact that MGr3 exhibits a lower porosity compared to that of the physical mixture must be related to the relatively high porosity of Gr3. Indeed, since Gr3 is porous, MOF units may deposit inside its pores and thus decrease the porosity of the hybrid materials compared to what would be expected for a simple juxtaposition of the MOF and graphite "phases". This is supported by the fact that Gr3 contains large volume of mesopores.

To confirm the limited number of functional groups on the surface of graphites hypothesized above, potentiometric titrations were performed. The results are presented in Table 2. The functional groups detected are classified as relatively strong acidic groups ($pK_a < 7$) or weak acidic groups ($pK_a > 7$). As expected, the graphites have negligible amount of oxygen acidic groups compared to GO.[38] The exception is exfoliated graphite (Gr5) which has about three times less groups than GO. These results support our hypothesis that graphites, unlike GO, cannot form linkages with the MOF (at least not to a significant extent). Moreover, Gr5, which has a relatively high amount of oxygen groups, exhibits higher porosity than the other hybrid materials. Nevertheless, the low content of graphite in Gr5 can also contribute to this result.

Additional information on the structure of the materials is provided by Raman spectroscopy. The spectra for the parent materials and the hybrid materials are presented in Figure 3. As expected, two bands are observed on the spectra of the graphite samples: one at 1585 cm^{-1} (G band) and another at 1360 cm^{-1} (D band).[39,40] The former one represents the in-phase vibration of the graphite lattice, whereas the latter band indicates the

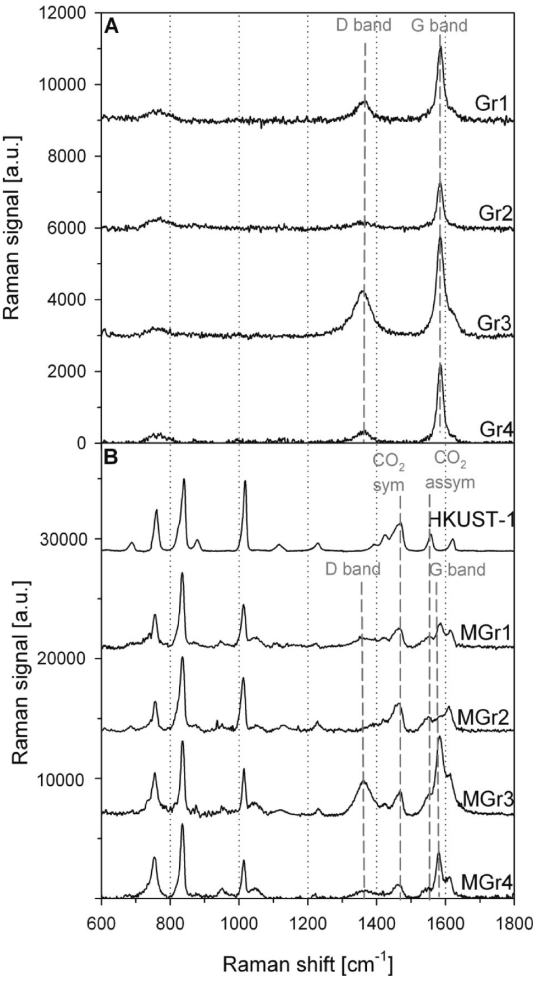

Figure 3. Raman spectra for the graphite samples (A) and HKUST-1 and the hybrid materials.

presence of disordered regions/defects in the graphite lattice and may be the result of the physical process undertaken by the materials (e.g., milling, grinding).[39,40] The intensity ratio of the bands at 1585 and 1360 cm^{-1} provides an indication of the disorder in the material studied.[39] Lower numbers represent higher degree of disorder. The values of this ratio are 4.0, 8.6, 2.0, and 12.2 for Gr1, Gr2, Gr3, and Gr4, respectively. This indicates that Gr1 and Gr3 are the most disordered materials whereas Gr2 and Gr4 exhibit fewer defects. This is in agreement with the conclusions drawn from XRD measurements. Several bands are observed on HKUST-1 spectrum with the most predominant ones at 1610, 1550, and 1460 cm^{-1}. These band positions are in accordance with the ones reported in the literature for this MOF (± 2 cm^{-1}) and correspond to the C═C, C−O_2 (asymmetric), and C−O_2 (symmetric) vibrations, respectively.[35] The spectra of the hybrid materials exhibit the features of both graphite and HKUST-1, confirming the presence of both "phases". In spite of the overlap around 1600 cm^{-1}, a trend can be noticed: the intensities at 1460 cm^{-1} and 1550 cm^{-1}, corresponding to the CO_2 symmetric and asymmetric stretching vibrations respectively, are less intense in the composites than in pure MOF. In addition to that, the intensity of those vibrations is smaller for flakes' sizes below 10 μm than for flakes' sizes above 10 μm. Conversely, there is no trend in the intensity of the C═C ring

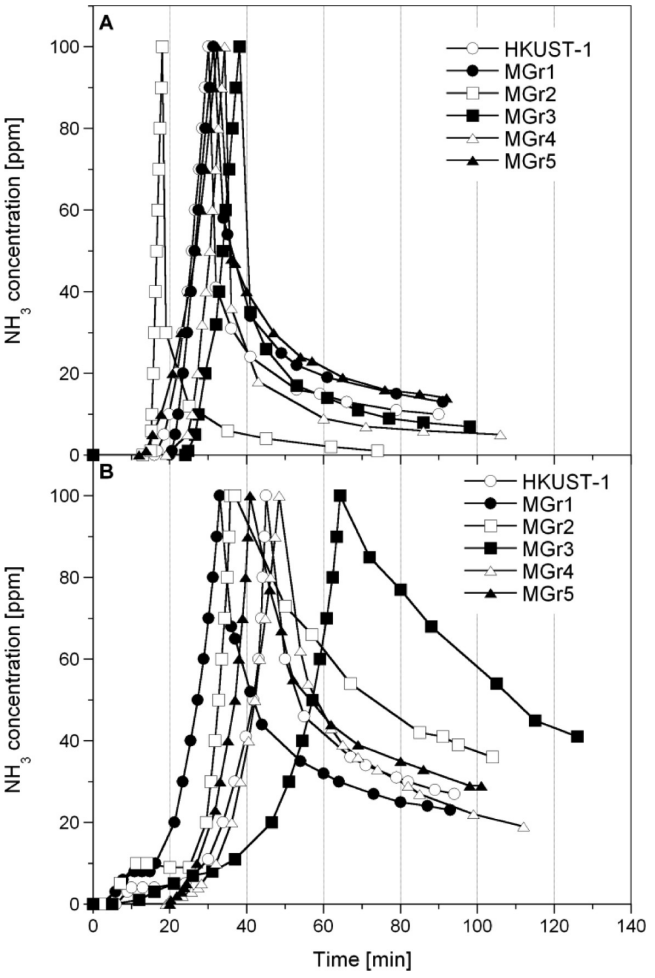

Figure 4. Ammonia breakthrough and desorption curves for the samples studied in (A) dry and (B) moist conditions.

stretching mode with a flake size. Our attempt is to link the degree of distortion in the MOF structure to the trend in spectral intensity for the CO_2 stretching vibrations. Indeed, the carboxylate functionalities are at the junctions with the metallic ions. Consequently, any change in these bands is a sign of a change in the framework's connections and thus its stability. In our case, the decrease of the CO_2 vibration intensity indicates a greater distortion. Considering all of these, the observed trend suggests that the smaller flakes are detrimental in the formation of "perfect" MOF units. This can be explained by the fact that small flakes disturb the synthesis of large units of MOF. More precisely, in the case of small flakes, the surface contact between the graphite component and the MOF is increased compared to the case of larger flakes. Consequently, increased hindrance/disturbance exists in the case of small flakes, which leads to greater distortion. Such analysis is valid if we consider the resonance effect from the laser minimal and equivalent for all samples. This condition is likely met since composites' absorption at the laser excitation is low and the absorption and therefore resonance contributions to the Raman intensities should be the same for all composite samples.[35]

The flakes' size seems to impact the porosity of the materials as well. We observe that overall, the percentage of the decrease in surface area compared to HKUST-1 is more pronounced with a decrease in the graphite flake size. Once again, this must be related to the greater surface contact between MOF and the graphite in the case of small flakes. It must be noted that Gr5 is not considered here as it contains much less graphite than the other materials and besides, we have seen that the presence of functional groups on its surface significantly modifies its structure compared to the other hybrid materials. This trend is in agreement with the one described above with Raman spectra. Indeed, since MOF units are those responsible for porosity, more defects/distortion in this phase result in smaller surface area.

Table 3. Ammonia Breakthrough Capacities Measured and Calculated for the Physical Mixture for the Samples Studied

	NH_3 breakthrough capacity [mg/g]	breakthrough capacity of the physical mixture [mg/g]
HKUST-1-ED	87	
HKUST-1-EM	133	
MGr1-ED	84	78
MGr1-EM	97	119
MGr2-ED	51	78
MGr2-EM	105	120
MGr3-ED	64	77
MGr3-EM	108	118
MGr4-ED	66	74
MGr4-EM	90	113
MGr5-ED	92	84
MGr5-EM	118	128

Ammonia removal from air was tested on the parent and hybrid materials in dynamic conditions and at room temperature. The breakthrough and desorption curves are plotted in Figure 4. It is important to note that the tests were not carried out until whole breakthrough sigmoidal curves were recorded. The breakthrough was monitored until the outlet concentration reached 10% of the inlet concentration, and thus only a rapid increase in the ammonia concentration is observed up to 100 ppm. The decrease in concentration observed afterward corresponds to the desorption curve. During that step, no more ammonia is injected in the system and only air passes through the adsorbent's fixed bed. This part enables to assess the amount of ammonia released and thus to evaluate the strength of ammonia retention. The steeper the desorption curve, the smaller the amount of ammonia desorbed and thus the stronger the retention process. HKUST-1 and the hybrid materials tested in the dry conditions exhibit steep breakthrough and desorption curves, which indicate the fast kinetics of interactions and the strong adsorption of ammonia, respectively. In the moist conditions however, the desorption curves are much less steep which suggests the weaker retention of ammonia. This has already been observed in the case of MOF/GO composites and attributed to the presence of ammonia dissolved in water.[25] This type of ammonia is easily removed during air purging together with water vapor phase.

The breakthrough capacities, derived from the breakthrough curves, are listed in Table 3. While graphite samples are known to be very poor ammonia adsorbents,[27,33] the high adsorption capacities were reported on HKUST-1.[25,41−43] The performance of the hybrid materials is similar to or lower than that of HKUST-1. It is important to mention that the measured adsorption capacities are in the range (difference of less than 10%) or lower than those calculated for the physical mixture of HKUST-1 and

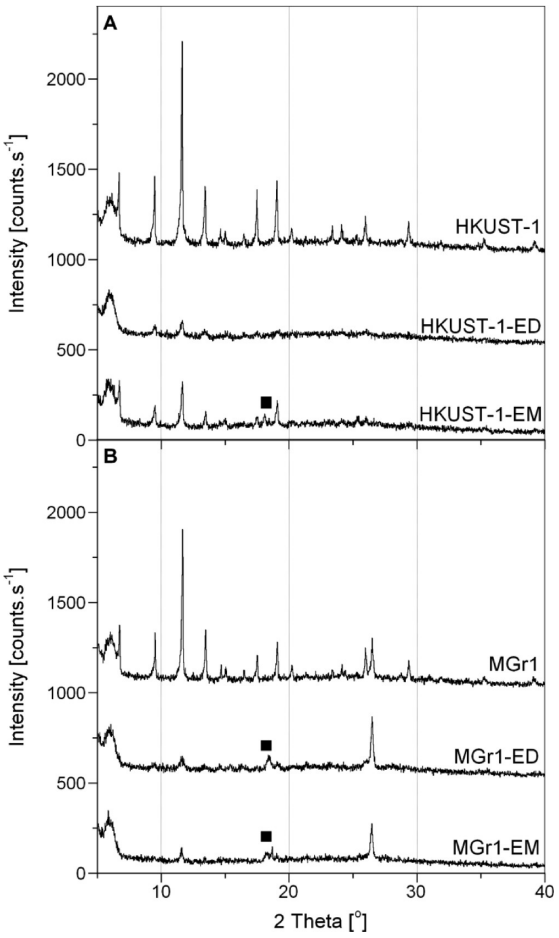

Figure 5. XRD patterns for HKUST-1 (A) and MGr1 (B) before and after exposure to ammonia with evidence of a new peak (■).

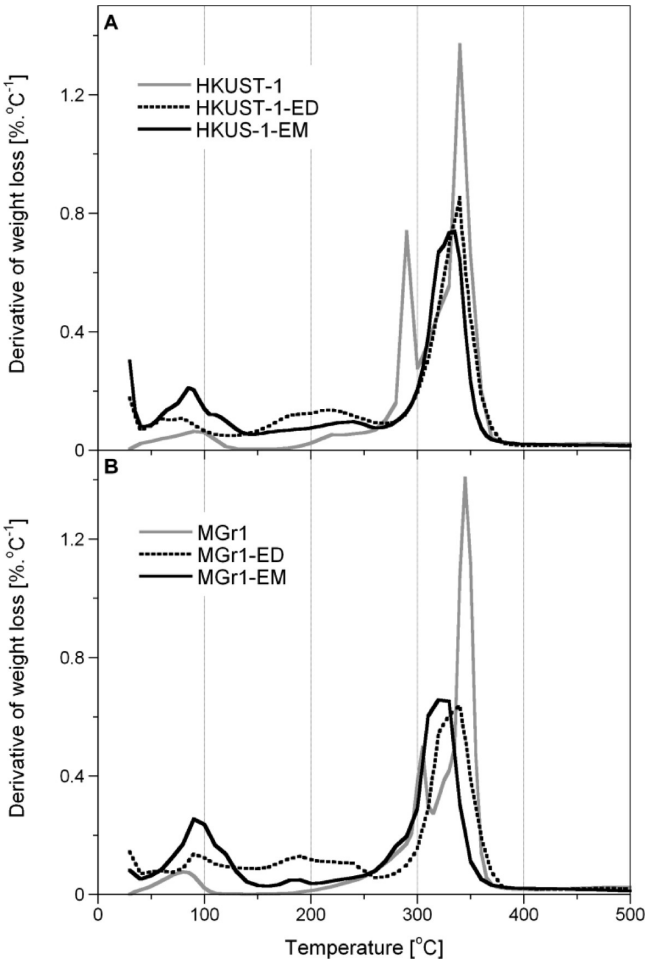

Figure 6. DTG curves for HKUST-1 (A) and MGr1 (B) before and after exposure to ammonia.

graphite (see Table 3). These calculations were done considering the nil adsorption capacity of the graphite samples. The fact that the measured adsorption capacities are lower than those calculated for a hypothetical physical mixture might seem unexpected at the first glance. For an "ideal" physical mixture, one would a priori expect them to be equal. Indeed, in such a case, both HKUST-1 and the graphite would be as they are in the separated case, and the adsorption capacity of the resulting hybrid material should be equal to the addition of the corresponding capacity of MOF and GO taking into account the percentage of each of them. This is not the case for our materials. Since, the graphite component has affected the formation of the MOF as described previously (see SEM micrographs in Figure 2), the HKUST-1 "phase" in the hybrid materials is not the same as in HKUST-1 "alone" or when physically mixed with graphite. Another explanation for the difference between measured and calculated adsorption capacities is the hydrophobic character of graphite. This feature likely reduces the apparent hydrophilicity of the MOF in the region close to the graphite component and thus has a negative impact on the ammonia adsorption capacity of the hybrid material.

The surface of the exhausted samples was analyzed in order to understand the mechanisms of adsorption. Since all the exhausted hybrid materials exhibited similar patterns typical for the MOF exposed to ammonia, only the results for one hybrid material (MGr1) are presented and compared to those for HKUST-1.

Figure 5 shows the XRD patterns of the samples before and after exposure to ammonia. Ammonia adsorption visibly causes the collapse of the MOF structure in both HKUST-1 "alone" and in the hybrid materials. This is demonstrated by the disappearance of the majority of peaks. This was anticipated considering the previous results obtained on MOF/GO composites.[25] As expected, the peak from the graphite component (at 2θ about 26.6°) remains on the pattern of the exhausted sample owing to its inert nature toward interactions with ammonia. However, it is interesting to note that a new peak at 2θ about 18° appears after exposure to ammonia in dry conditions for HKUST-1 and in dry and moist conditions for MGr1. This new peak must be related to the formation of a new species and has been already observed for the MOF/GO composites.[25]

The collapse of the MOF structure (in both HKUST-1 "alone" and in the hybrid materials) upon the exposure to ammonia is confirmed by thermogravimetric analysis (Figure 6). The temperature range above 500 °C is not displayed as no features were revealed in this range. A first peak at about 100 °C observed on DTG curves for the initial samples corresponds to the removal of solvent.[43] Then the decomposition of the MOF occurs starting at about 300 °C (decomposition of the ligand).[44] After the exposure to ammonia, a broadening of the peak at about 350 °C is observed. This weight loss corresponds to the decomposition of the organic ligand. The broadening for both the exhausted

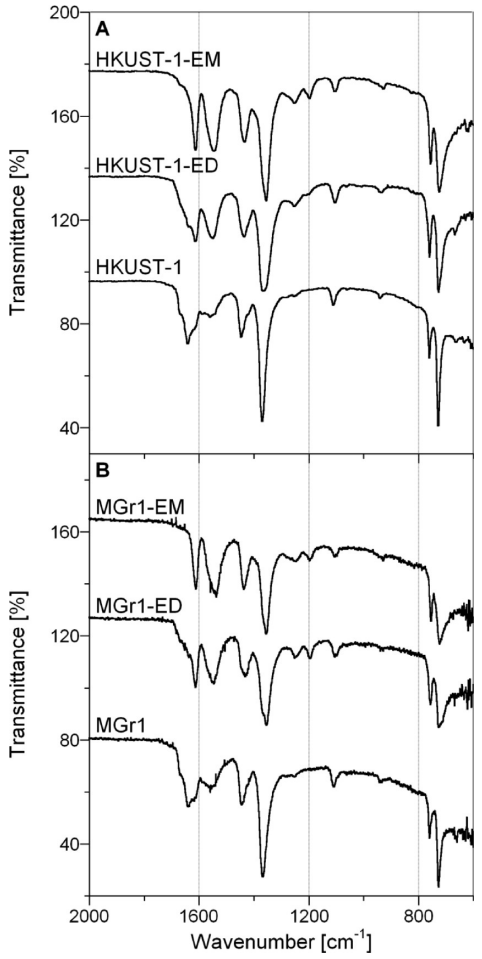

Figure 7. FT-IR spectra for HKUST-1 (A) and MGr1 (B) before and after exposure to ammonia.

HKUST-1 sample and the hybrid materials, in comparison to the initial samples, indicates that the ligands were released from the MOF structure (not coordinated to the copper units).[25] Besides these features, the intensity of the peak at about 90 °C increased and a shoulder appeared at about 115 °C for the samples run in moist conditions. We linked this to the removal of different types of water: the one adsorbed physically and the one previously coordinated to the copper centers of the MOF. The broad peak observed between 150 and 250 °C is more pronounced in dry conditions and indicates the presence of new species. Based on the chemistry of the materials described here and on the results of the previous studies, this peak is assigned to the decomposition of $Cu(OH)_2$ and/or $Cu(NH_3)_4^{2+}$ and/or to the release of strongly adsorbed ammonia.[45,46]

The FT-IR spectra of the materials before and after ammonia adsorption are reported in Figure 7. Only the range 600—2000 cm^{-1} is displayed since the minor features are revealed at higher wavenumbers. The initial spectra for HKUST-1 and MGr1 exhibit several bands assigned to the symmetric (1370 and 1450 cm^{-1}) and asymmetric (1590 and 1645 cm^{-1}) vibrations of the carboxylate groups of the BTC ligand.[47,48] Below 1300 cm^{-1}, out of plane vibrations of the organic ligand are seen. As expected, the FT-IR spectra of all graphite samples do not show any bands. After exposure to ammonia, changes in the spectra of the samples are observed. Briefly, for both HKUST-1 and MGr1 run in dry and moist conditions, new bands appear at ~1620, 1260, and 1210 cm^{-1} and a broadening of the bands at 1450, 1370, and 730 cm^{-1} with an increase in the intensity of the band at about 1560 cm^{-1} are observed. As described in detail in a previous study,[24] these changes are related to a change in the coordination of the carboxylate organic ligands caused by their progressive release from the copper sites (release of BTC).[22,48,49] These findings support the results of thermal analyses detailed above.

Depending on the type of application targeted, the unstability of the MOF may or may not be an issue. When dealing with MOF materials, a trade-off between chemical stability and adsorption capacity (and strength) must often be made. Indeed, when only physisorption is involved at ambient conditions, the amount of gas adsorbed in often limited and the strength of retention is weak thus resulting in a progressive release of the gas. However, no collapse of the MOF is observed. On the contrary, when reactive adsorption/chemisorption is involved, as it is the case in this study, the targeted species interact strongly with the adsorbent and thus they are not released from the surface. Nevertheless, these strong interactions can significantly impair the stability of the material, and a collapse of the structure can be observed. When the potential application of the adsorbents is in respirators filters for toxic species the high capacity and strong adsorption are of paramount importance. Even though the adsorbent is not stable upon exposure to adsorbate Examples of MOF exhibiting stronger stability upon exposure to ammonia include MIL-100(Fe) and COF-10.[50,51] Nevertheless their capacity as filtration media is lower.

CONCLUSIONS

The results of this study indicate that the oxidation of graphite is important to build MOF/graphite hybrid materials with synergistic properties. The presence of functional groups on the substrate's surface enables the formation of bonds between the components and thus the composites can be formed. The results suggest that MOF/graphite hybrid materials represent a distorted physical mixture of MOF and graphite. Besides the chemical features of the graphites, the physical parameters, and especially the porosity and size of flakes, also seem to influence the formation of the hybrid materials. Overall, the graphite particles interfere with the formation of HKUST-1 and induce a different crystal morphology (more defects and increased surface roughness) than the one observed when MOF is formed in the absence of a substrate. The latter behavior causes that less ammonia is adsorbed on the hybrid materials than what would be expected from the simple physical mixture of HKUST-1 and graphite. As already described in previous studies, ammonia adsorption induces the collapse of the MOF structure and changes in the chemistry of materials, in both HKUST-1 and the hybrid materials.

ASSOCIATED CONTENT

Supporting Information. Nitrogen isotherms for HKUST-1 and the hybrid materials. This material is available free of charge via the Internet at http://pubs.acs.org.

AUTHOR INFORMATION

Corresponding Author

*Fax: +1 212-650-6107. E-mail: tbandosz@ccny.cuny.edu.

■ ACKNOWLEDGMENT

This work was supported by ARO (Army Research Office) Grant W911NF-10-1-0030 and NSF collaborative Grant 0754945/0754979.

■ REFERENCES

(1) Czaja, A. U.; Trukhan, N.; Muller, U. *Chem. Soc. Rev.* **2009**, *38*, 1284–1293.
(2) Müller, U.; Schubert, M. M.; Yaghi, O. M. In *Chemistry and Applications of Porous Metal−Organic Frameworks, Handbook of Heterogeneous Catalysis*; Müller, U., Schubert, M. M., Yaghi, O. M., Eds.; Wiley-VCH Verlag GmbH & Co. KGaA: Weinheim, Germany, 2008; p 247−262.
(3) Li, J.-R.; Kuppler, R. J.; Zhou, H.-C. *Chem. Soc. Rev.* **2009**, *38*, 1477–1504.
(4) Wright, P. *Microporous framework solids*; RSC Publishing: Cambridge, U.K., 2008.
(5) James, S. L. *Chem. Soc. Rev.* **2006**, *32*, 276–288.
(6) Horcajada, P.; Serre, C.; Vallet-Regí, M.; Sebban, M.; Taulelle, F.; Férey, G. *Angew. Chem., Int. Ed.* **2006**, *118*, 6120–6124.
(7) Chen, B.; Wang, L.; Zapata, F.; Qian, G.; Lobkovsky, E. B. *J. Am. Chem. Soc.* **2008**, *30*, 6718–6719.
(8) Chen, B.; Wang, L.; Xiao, Y.; Fronczek, F. R.; Xue, M.; Cui, Y.; Qian, G. *Angew. Chem., Int. Ed.* **2009**, *48*, 500–503.
(9) Lan, A.; Li, K.; Wu, H.; Olson, D. H.; Emge, T. J.; Ki, W.; Hong, M.; Li, J. *Angew. Chem., Int. Ed.* **2009**, *48*, 2334–2338.
(10) Mahata, P.; Natarajan, S.; Panissod, P.; Drillon, M. *J. Am. Chem. Soc.* **2009**, *131*, 10140–10150.
(11) Harbuzaru, B. V.; Corma, A.; Rey, F.; Jordá, J. L.; Ananias, D.; Carlos, L. D.; Rocha, J. *Angew. Chem., Int. Ed.* **2008**, *47*, 1080–1083.
(12) Arnold, M.; Kortunov, P.; Jones, D. J.; Nedellec, Y.; Kärger, J.; Caro, J. *Eur. J. Inorg. Chem.* **2007**, *2007*, 60–64.
(13) Gascon, J.; Aguado, S.; Kapteijn, F. *Microporous Mesoporous Mater.* **2008**, *113*, 132–138.
(14) Liu, Y.; Ng, Z.; Khan, E. A.; Jeong, H.-K.; Ching, C.-B.; Lai., Z. *Microporous Mesoporous Mater.* **2009**, *118*, 296–301.
(15) Yoo, Y.; Jeong, H.-K. *Chem. Commun.* **2008**, *2008*, 2441–2443.
(16) Hermes, S.; Zacher, D.; Baunemann, A.; Wöll, C.; Fischer, R. A. *Chem. Mater.* **2007**, *19*, 2168–2173.
(17) Gorka, J.; Fulvio, P. F.; Pikus, S.; Jaroniec., M. *Chem. Commun.* **2010**, *46*, 3798–6800.
(18) Furtado, A. M. B.; Liu, J.; Wang, Y.; LeVan, M. D. *J. Mater. Chem.* **2011**, *21*, 6698–6706.
(19) Shekhah, O.; Roques, N.; Mugnaini, V.; Munuera, C.; Ocal, C.; Veciana, J.; Woll, C. *Langmuir* **2008**, *24*, 6640–6648.
(20) Jahan, M.; Bao, Q.; Yang, J.-X.; Loh, K. P. *J. Am. Chem. Soc.* **2010**, *132*, 14487–14495.
(21) Petit, C.; Bandosz, T. J. *Adv. Mater.* **2009**, *21*, 4753–4757.
(22) Petit, C.; Bandosz, T. J. *Carbon* **2011**, *49*, 563–572.
(23) Petit, C.; Bandosz, T. J. *J. Mater. Chem.* **2009**, *19*, 6521–6528.
(24) Petit, C.; Bandosz, T. J. *Adv. Funct. Mater.* **2010**, *20*, 111–118.
(25) Petit, C.; Mendoza, B.; Bandosz, T. J. *Langmuir* **2010**, *26*, 15302–15309.
(26) Chui, S. S.-Y.; Lo, S. M.-F.; Charmant, J. P. H.; Orpen, A. G.; Williams, I. D. *Science* **1999**, *283*, 1148–1150.
(27) Seredych, M.; Tamashausky, A. V.; Bandosz, T. J. *Carbon* **2008**, *46*, 1241–1252.
(28) Morishige, K.; Hamada, T. *Langmuir* **2005**, *21*, 6277–6281.
(29) Brunauer, S.; Emmett, P. H.; Teller, E. *J. Am. Chem. Soc.* **1938**, *60*, 309–319.
(30) de Boer, J. H.; Lippens, B. C.; Linsen, B. G.; Broekhoff, J. C. P.; van den Heuvel, A.; Osinga, T. J. *J. Colloid Interface Sci.* **1966**, *21*, 405–414.
(31) Jagiello, J. *Langmuir* **1994**, *10*, 2778–2785.
(32) Jagiello, J.; Bandosz, T. J.; Schwarz, J. A. *Carbon* **1994**, *32*, 1026–1028.
(33) Seredych, M.; Petit, C.; Tamashausky, A. V.; Bandosz, T. J. *Carbon* **2009**, *47*, 445–456.
(34) Milev, A.; Wilson, M.; Kannangara, G. S. K.; Tran, N. *Mater. Chem. Phys.* **2008**, *111*, 346–350.
(35) Prestipino, C.; Regli, L.; Vitillo, J. G.; Bonino, F.; Damin, A.; Lamberti, C.; Zecchina, A.; Solari, P. L.; Kongshaug, K. O.; Bordiga., S. *Chem. Mater.* **2006**, *8*, 1337–1346.
(36) Cai, D.; Song., M. *J. Mater. Chem.* **2007**, *17*, 3678–3680.
(37) Spokoyny, A. M.; Kim, D.; Sumrein, A.; Mirkin, C. A. *Chem. Soc. Rev.* **2009**, *38*, 1218–1227.
(38) Petit, C.; Bandosz, T. J. *J. Phys. Chem. C* **2009**, *113*, 3800–3809.
(39) Tuinstra, F.; Koenig, J. L. *J. Chem. Phys.* **1970**, *53*, 1126–1130.
(40) Kudin, K. N.; Ozbas, B.; Schniepp, H. C.; Prud'homme, R. K.; Aksay, I. A.; Car, R. *Nano Lett.* **2008**, *8*, 36–41.
(41) Peterson, G. W.; Wagner, G. W.; Balboa, A.; Mahle, J.; Sewell, T.; Karwacki, C. J. *J. Phys. Chem. C* **2009**, *113*, 13906–13917.
(42) Britt, D.; Tranchemontagne, D.; Yaghi, O. M. *Proc. Natl. Acad. Sci. U.S.A.* **2008**, *105*, 11623–11627.
(43) Thomas, K. M. *Dalton Trans.* **2009**, *2009*, 1487–1505.
(44) Seo, Y.-K.; Hundal, G.; Jang, I. T.; Hwang, Y. K.; Jun, C. H.; Chamg, J. H. *Microporous Mesoporous Mater.* **2009**, *119*, 331–337.
(45) Liu, N.; Wu, D.; Wu, H.; Luo, F.; Chen, J. *Solid State Sci.* **2008**, *10*, 1049–1055.
(46) Selim, S. A.; Hassan, H. A.; Abd-El-Khalik, M.; Mikhail, R. S. *Thermochim. Acta* **1981**, *45*, 349–360.
(47) Vairam, S.; Govindarajan, S. *Thermochim. Acta* **2004**, *414*, 263–270.
(48) Nakamoto, K. In *Infrared and Raman Spectra of Inorganic and Coordination Compounds, Applications in Coordination, Organometallic, and Bioinorganic Chemistry*; John Wiley & Sons: Hoboken, NJ, 2009; pp 62−67.
(49) Shi, N.; Yin, G.; Han, M.; Jiang, L.; Xu, Z. *Chem.—Eur. J.* **2008**, *14*, 6255–6259.
(50) Petit, C.; Bandosz, T. J. *Adv. Funct. Mater.* **2011**, *21*, 2108–2117.
(51) Doonan, C. J.; Tranchemontagne, D. J.; Glover, T. G.; Hunt, J. R.; Yaghi, O. M. *Nat. Chem.* **2010**, *2*, 235–238.